Hindawi
Indoor Air
Volume 2023, Article ID 3605937, 15 pages
https://doi.org/10.1155/2023/3605937

Research Article

Combining Chamber Experiments and Model Simulations to Evaluate an Indoor HONO Source with Surface Photochemical Properties

Youfeng Wang[1,2] **Chong Zhang**[1] **Jianshu Wang**[1] **Yaru Wang**[1] **Yingjie Zhang**[1,3] **Weili Lin**[4] **and Chunxiang Ye**[1]

[1]*SKL-ESPC & SEPKL-AERM, College of Environmental Sciences and Engineering, and Center for Environment and Science, Peking University, Beijing 100871, China*
[2]*Beijing Municipal Ecological and Environmental Monitoring Center, Beijing, China*
[3]*School of Ecology and Nature Conservation, Beijing Forestry University, Beijing 100083, China*
[4]*College of Life and Environmental Sciences, Minzu University of China, Beijing, China*

Correspondence should be addressed to Chunxiang Ye; c.ye@pku.edu.cn

Received 11 March 2023; Revised 5 September 2023; Accepted 8 September 2023; Published 6 October 2023

Academic Editor: Geun Young Yun

Nitrous acid (HONO) is an emerging indoor pollutant that can exert adverse health effects. The chemical production of indoor HONO has been attributed to NO_2 heterogeneous reactions, and the source strength has been extensively evaluated via laboratory and model simulation studies. Photolysis of surface nitrate has recently been proposed as an indoor HONO source based on correlation analysis between indoor HONO accumulation and visible light radiation. However, neither experimental validation of the proposed mechanism nor source strength characterization is currently available. In this work, we designed an outdoor photochemical chamber (OPC) to simulate indoor HONO accumulation and established an indoor photochemical model (ICM) to calculate the indoor HONO budget. Indoor HONO accumulation revealed a distinct diel variation with a daytime maximum. Only with this indoor HONO source, the ICM reproduced the indoor HONO budget determined in the OPC. The enhanced reactive cross section of surface nitrate in visible light accounted for the major portion of the HONO source budget (77.2%) and the distinct diel variation. Success with the ICM encouraged us to simulate the HONO budget in real indoor environments. The calculated HONO production rates from surface nitrate photolysis at noon ranged from 1.4 to 4.1 ppbv h^{-1} under different indoor scenarios. On a daily average, this indoor HONO source contributed 42.4–52.7% to the total chemical sources in the living room but only contributed 4.7% to that in the kitchen, where NO_2 heterogeneous reactions dominated.

1. Introduction

From air quality and human health perspectives, the indoor environment is worthy of much more research attention as a highly frequented living environment for residents [1]. Indoor air is influenced by outdoor air pollutant inputs and indoor sources and hence could notably differ from outdoor air [2]. Deep concern on indoor air quality led us to research areas involving indoor sources or indoor physical and chemical processes that control the distribution of both gaseous and particulate pollutants.

Compared to the outdoor atmosphere, the indoor environment features a high surface area to volume (S/V) ratio [3] and low ultraviolet (UV) radiation [4, 5]. As such, surface reactions of (semi)volatile organic and inorganic compounds have drawn intensive research attention [6–9]. Scientists have treated indoor surfaces as surface reservoirs containing chemical constituents subject to exchange with

the gas phase. Several groups have obtained measurements on the release of volatile organic compounds and nitrous acid (HONO) from indoor surfaces and have identified corresponding sources [10–12]. Adopting HONO as an example, the surface nitrite reservoir is 1–2 orders of magnitude more abundant than the indoor HONO [10]. Changes in room temperature or indoor HONO concentration can lead to repartitioning between the surface nitrite reservoir and indoor HONO [10, 12]. The ultimate sources of HONO or surface nitrite include direct emissions from combustion processes and surface reactions. Burning candles, gas stoves, cigarette smoking, and open fireplaces [13] are presumably the major emission sources. A major indoor chemical source of HONO is associated with the photoenhanced heterogeneous reaction of NO_2 on various indoor surfaces [14–17]. The HONO production from NO_2 surface reactions and its response with the relative humidity (RH) have been consistently observed under indoor irradiation [14]. Knowledge of the relationship between HONO production rate and NO_2 concentration under different light intensities (Table S1 and references therein [14, 15, 18–29]) facilitates the parameterization of the photoenhanced uptake coefficient of NO_2 (γ, as expressed in equation (1) in kinetic models.

$$\gamma = \gamma_0 \times \mathrm{EF}. \quad (1)$$

EF is the uptake enhancement factor under a defined light density relative to dark conditions (γ_0), which is vital for the evaluation of the HONO production from photoenhanced NO_2 surface reactions.

A novel chemical source of indoor HONO in discussion is the photolysis of surface nitrate. Schwartz-Narbonne et al. measured HONO release employing several indoor lamps and proposed the photolysis of nitrate absorbed on painted walls as a novel indoor HONO source [30]. However, neither the detailed reaction mechanism nor the reaction rate has been examined. A similar proposal of enhanced nitrate photolysis on snow/ice surfaces has introduced the concept of a quasiliquid layer (QLL) on snow/ice surfaces, which allows the coexistence of quasiliquid water, nitrate, and organic matter absorbed on surfaces [31]. Later, enhanced photolysis of nitrate on aerosol particle surfaces and other ambient surfaces, such as tree leaves, has also been confirmed in several laboratory studies, with a rate determined by the nitrate surface density [32–37]. Scientists have employed the concept of catalytic surface films and surface catalysis mechanisms to describe the dependence of the photolysis rate on the nitrate surface density or nitrate surface coverage [32–34, 37]. Although the microphysicochemical properties of the QLL and surface films have not been comprehensively and quantitatively characterized, they are analogous to a certain extent, namely, these films preserve nitrate in a similar but particular state far from being isolated, which might be the key reason for the catalyzed photolysis of surface nitrate [36–39]. Svoboda et al. calculated the absorption spectrum of bare nitrate anions and nitrate–water clusters, confirming a shift in the 300 nm absorption band depending on the number of water molecules [40]. In laboratory, researchers have also measured a redshift in the absorption spectra of nitrate on silicon surfaces [41, 42] and HNO_3/NO_3^- on sapphire window surfaces [43], in the 290–365 nm range. Recently, we measured and reported the enhanced and redshifted reactive cross section of nitrate on aerosol particles with the enhanced absorption spectrum extending from 365 to 605 nm [44]. These measurements added key information on the surface catalysis mechanism, i.e., more overlap between the absorption spectrum of surface-absorbed nitrate and light spectrum could lead to increased HONO production via enhanced photolysis of surface nitrate powered by both UV and visible light under solar radiation or indoor lighting. It is likely that the contribution of longer wavelengths in UV or even visible light might cause indoor HONO accumulation. One reason is the increased HONO production beyond 300 nm as a result of the enhancement in both the absorption cross section and photon flux at longer wavelengths. Another reason is the dependence of HONO photolysis on UV light with wavelengths shorter than 400 nm [45], which is either mostly filtered by windows or not emitted by indoor lamps. Hence, the presumed consequence is enhanced production and suppressed photolysis loss leading to an inevitable accumulation of indoor HONO. With absorption cross section and photolysis rate available, our assumption can be quantitatively evaluated in a similar experiment to that of Schwartz-Narbonne et al. [30].

The indoor surface reactions producing HONO could be simplified as a two-step process, i.e., chemical production of nitrite on the surface, which is followed by partitioning and diffusion within the surface and bulk and gas phases. When the chemical production of nitrite dominates, partitioning and diffusion do not influence the immediate HONO yield resulting from photoenhanced NO_2 heterogeneous reactions [14]. The HONO production from either the photolysis of surface-absorbed nitrate or photoenhanced NO_2 heterogeneous reactions on aerosol particle surfaces highly depends on the light intensity [14, 34], suggesting a robust linkage between nitrite chemical production and the immediate HONO yield. Therefore, the HONO production rate, P_{HONO} as described in the fundamental photochemistry, can be defined in equation (2) as follows:

$$P_{\mathrm{HONO}} = \int N_{rp} I(\lambda) \sigma(\lambda) \varnothing(\lambda) d\lambda, \quad (2)$$

where N_{rp}, $I(\lambda)$, $\sigma(\lambda)$, and $\varnothing(\lambda)$ denote the reactant pollutant (surface-absorbed nitrate) amount, light spectrum, absorption cross section or absorption spectrum of surface pollutants, and corresponding quantum yield of the photochemical product (HONO in this case), respectively. The surface-absorbed nitrate amount and actinic flux could be directly measured in the real indoor environment. To evaluate the indoor HONO production, the product of the absorption cross section of surface-absorbed nitrate and the corresponding quantum yield of HONO at each wavelength refers to our recent laboratory-determined reactive cross

section of surface-absorbed nitrate [44], $\sigma_{re}(\lambda)$ (equation (3)), which can be obtained as follows:

$$\sigma_{re}(\lambda) = \sigma(\lambda)\varnothing(\lambda). \quad (3)$$

With laboratory-determined $\sigma_{re}(\lambda)$, reasonable evaluation of this indoor HONO source is practical.

In this study, an outdoor photochemical chamber (OPC) with painted wall (Dulux latex paint) and regulating ventilation was built to simulate an enclosed room. HONO accumulation was directly monitored as a function of surface photochemical aging and illumination. An indoor photochemical model (ICM) summarizing surface-absorbed nitrate photolysis, photoenhanced NO_2 heterogeneous reactions, and other HONO budget terms, i.e., HONO ventilation and photolysis losses, was constructed to simulate the HONO accumulation and budget in our OPC experiment. Reproduction of HONO accumulation in the OPC could facilitate further application of the ICM in the evaluation of this HONO source in real indoor environments. The environmental variation in this indoor HONO source was characterized with the surface nitrate density and window transmission of the actinic flux as major influencing factors.

2. Materials and Methods

2.1. Outdoor Photochemical Chamber (OPC) Experiment. The configuration of our OPC is shown in Figure S1, and the dimensions of the OPC are summarized in Table S2. The OPC comprised a stainless-steel-structured cubic reactor with a side length of 0.5 m and S/V ratio of 12 m^{-1}. The chamber interior walls except for the roof were painted white (paint brand: Dulux) to simulate the painted wall surfaces in households, and the external walls were covered with thermal insulation materials and wood. The chamber roof consisted of a UV-cutoff glass filter to mimic indoor lighting conditions [46]. The glass filter provided a high transmittance of 89% at 500 nm with a cutoff wavelength of 425 nm (Figure S2). The OPC was equipped with a gas inlet system and a measurement system. The gas inlet system allowed flow control through a set of mass flow controllers and could deliver either ambient air, zero air, or laboratory mixing air into the chamber. A modified long-path absorption photometric (LPAP) instrument was used to measure the HONO and NO_2 levels in the chamber at a total sampling rate of 0.8 L min^{-1}. The measurement detection limits for HONO and NO_2 reached 3 and 9 pptv, respectively, with a precision within 25% [44].

Ventilation, surface properties, lighting conditions, and NO_2 concentration are major influencing factors, and these parameters were therefore adopted as control factors in this OPC experiment. The OPC experiments were performed under a ventilation flow of 1.0 L min^{-1} (or a ventilation rate of ca. 0.48 h^{-1}) to maintain a slight positive pressure in the chamber and to prevent air permeation from the ambient air. Before each experiment, the dormant window was maintained open to allow air exchange, indoor aerosol particle deposition, and HNO_3 partitioning. A chamber aged for half a year was used to simulate indoor wall surfaces. In the lighting control experiment, LED lamps, and solar radiation were compared. When LED lamps (5 W) were employed as light sources, the OPC chamber was placed in a dark environment, and HONO accumulation was monitored as the LED lamps were turned on or off. When solar radiation was employed as the light source, the OPC chamber was placed outdoors at the Peking University (PKU; 39.99°N, 116.30°E) site approximately 27 m above ground level. The solar spectrum and photolysis frequencies of HONO and NO_2 were measured via a charge-coupled device (CCD) spectrometer (Figure S3). In NO_2 concentration control design, parallel experiments with low- and high-NO_2 input airflows were conducted. Low-NO_2 air was generated by passing ambient air through glass tubes packed with potassium permanganate ($KMnO_4$) pellets and activated carbon, followed by a sodium carbonate (Na_2CO_3) denuder to remove reactive nitrogen species, including NO_x, HONO, and HNO_3. High-NO_2 air was generated by passing ambient air through the Na_2CO_3 denuder to remove only HONO and HNO_3. In each experiment, the HONO and NO_2 concentrations in the OPC and ambient air were simultaneously monitored.

2.2. Data Processing for the OPC Experiment. The HONO accumulation rate (in ppbv h^{-1}) resulting from surface nitrate photolysis in the OPC, $d[\mathrm{HONO}]_{snp}/\mathrm{dt}$, can be obtained from measurements of the raw HONO accumulation rate, $d[\mathrm{HONO}]_{indoor}/dt$.

$$\frac{d[\mathrm{HONO}]_{indoor}}{\mathrm{dt}} = \mathrm{HONO\ source} - \mathrm{HONO\ sink}, \quad (4)$$

$$\mathrm{HONO\ source} = \frac{\mathrm{d}[\mathrm{HONO}]_{snp}}{\mathrm{dt}} + \frac{\mathrm{d}[\mathrm{HONO}]_{NO_2}}{\mathrm{dt}} + F_{des}\frac{S}{V}, \quad (5)$$

$$\mathrm{HONO\ sink} = \frac{d[\mathrm{HONO}]_{ph}}{\mathrm{dt}} + \frac{\mathrm{d}[\mathrm{HONO}]_{vent}}{\mathrm{dt}} + F_{ads}\frac{S}{V}, \quad (6)$$

where $d[\mathrm{HONO}]_{NO_2}/\mathrm{dt}$, $d[\mathrm{HONO}]_{ph}/\mathrm{dt}$, and $d[\mathrm{HONO}]_{vent}/\mathrm{dt}$ denote the source or sink strength of the photoenhanced heterogeneous reactions of NO_2, HONO photolysis loss, and HONO ventilation loss, respectively, and F_{des} and F_{ads} are the HONO desorption and adsorption fluxes, respectively, representing the dynamic equilibrium between the surface nitrite reservoir and HONO.

$d[\mathrm{HONO}]_{NO_2}/\mathrm{dt}$ is the first-order reaction involving the NO_2 concentration and light intensity as primary kinetic assumptions, as expressed in

$$\frac{d[\mathrm{HONO}]_{NO_2}}{\mathrm{dt}} = \frac{1}{4} \times [\mathrm{NO_2}] \times 3600 \times \omega(\mathrm{NO_2}) \times \left(\frac{S - S_{shining}}{V} \times \gamma_0 + \frac{S_{shining}}{V} \times \gamma\right), \quad (7)$$

where $\omega(NO_2) = \sqrt{8\mathrm{RT}/\pi M}$ is the thermal velocity of NO_2, R is the ideal gas constant, T is the absolute temperature,

and M is the molecular mass of NO_2. $S_{shining}$ denotes the sunlit area in the OPC, which is twice the dormant window surface area, i.e., 0.5 m^2. The dependence of EF (enhancement factor of γ relative to γ_0) on the photolysis frequency of NO_2, j_{NO_2}, refers to the established linear relationship between EF and the light intensity [14, 20, 21, 25], as calculated with equation (8). EF is also depended on the initial NO_2 concentration, much higher in low-NO_x conditions than in high-NO_x conditions [14, 20, 21]. Parameterization of γ_0 and EF will be further discussed in Section 3.2.

$$\gamma = \gamma_0 \times \mathrm{EF} = \gamma_0 \times 6 \times \frac{j_{NO_2}}{j_{NO_2,\mathrm{noontime}}}. \quad (8)$$

$d[\mathrm{HONO}]_{ph}/dt$ can be determined via the HONO photolysis frequency, j_{HONO_indoor}, and mixing ratio (equation (9)). j_{HONO_indoor} can be calculated via an equation analogous to equation (2), as expressed in equation (10). The absorption cross-section of HONO and unit quantum yield can be referred to the JPL dataset [47].

$$\frac{d[\mathrm{HONO}]_{ph}}{dt} = j_{HONO\_indoor} \times [\mathrm{HONO}], \quad (9)$$

$$j_{HONO\_indoor} = \int I(\lambda)_{indoor} \sigma_{HONO}(\lambda) \varnothing_{HONO}(\lambda) d\lambda. \quad (10)$$

In the experiments with LED lamps as light sources, $I(\lambda)_{indoor}$ can be obtained from the LED emitting spectrum assuming that the light intensity is uniform in the OPC. In the experiments with solar radiation as the indoor light source, $I(\lambda)_{indoor}$ can be calculated with

$$I(\lambda)_{indoor} = I(\lambda) \times \mathrm{Transmittance}(\lambda), \quad (11)$$

where $I(\lambda)$ and $\mathrm{Transmittance}(\lambda)$ denote the outdoor solar spectrum and transmittance of the dormant window glass at the top of the OPC, respectively. The outdoor solar spectrum was recorded in real time with a CCD spectrometer during the OPC experiments.

The HONO ventilation loss ($d[\mathrm{HONO}]_{vent}/dt$) can be determined via the ventilation lifetime and the concentration gradient from the OPC to the ambient environment. The HONO concentration in the OPC should be much higher than that in the ambient environment. Therefore, the HONO ventilation loss can be simplified, as expressed in

$$\frac{d[\mathrm{HONO}]_{vent}}{dt} = [\mathrm{HONO}]_{indoor} \times k_{aer}, \quad (12)$$

where k_{aer} denotes the ventilation rate. As stated above, $d[\mathrm{HONO}]_{vent}/dt$ was set to $0.48 \times [\mathrm{HONO}]_{indoor}\ h^{-1}$ in the OPC experiment.

In our OPC experiment, the variation in HONO did not depend on the temperature (please refer to Section 3.1) in the daytime when HONO accumulation was remarkable, suggesting a slight effect of partitioning and diffusion on the various HONO budget terms [10, 48]. Assuming simultaneous equilibria between HONO and the surface nitrite reservoir, F_{des} and F_{ads} could be offset when adopting equations (5) and (6) (i.e., equation (4)) to calculate the raw HONO accumulation rate.

$d[\mathrm{HONO}]_{snp}/dt$ can finally be determined by combining all the information and equation (4)–(6). With knowledge of $d[\mathrm{HONO}]_{snp}/dt$, the HONO production flux in mole $m^{-2}\ h^{-1}$, F_{HONO}, in the OPC can be obtained with

$$\frac{d[\mathrm{HONO}]_{snp}}{dt} = F_{HONO} \times \frac{S_{shining}}{V}. \quad (13)$$

With knowledge of F_{HONO}, the HONO production rate in mole h^{-1} can be further defined as

$$P_{HONO} = F_{HONO} \times S_{Shining.} \quad (14)$$

Moreover, the photolysis rate constant of surface nitrate can be calculated with

$$j_{\mathrm{surface\ nitrate}} = \frac{P_{HONO}}{N_{nitrate}}, \quad (15)$$

where $N_{nitrate}$ denotes the abundance of surface nitrate (in mole) under exposure to lighting. Combining equations (2), (3), and (15), the reactive cross section of surface nitrate can finally be constrained (equation (16)) given the dependence of $\sigma_{re}(\lambda)$ on the surface nitrate density and the $\sigma_{re}(\lambda)$ profile previously measured [32, 37, 44].

$$j_{\mathrm{surface\ nitrate}} = \int_{\mathrm{cutoff}}^{605} I(\lambda)_{indoor} \sigma_{re}(\lambda) d\lambda. \quad (16)$$

Due to the lack of surface nitrate density ($D_{nitrate}$) measurements and the nonlinear relationship between $\sigma_{re}(\lambda)$ and $D_{nitrate}$ [32, 34, 37, 44], we assumed a certain $D_{nitrate}$ (or $N_{nitrate}$) value to obtain $j_{\mathrm{surface\ nitrate}}$. The range of indoor surface nitrate was reported to be varying from 10^{-3} to 10^{-5} mol m^{-2} [49]. An average $D_{nitrate}$ of 1.0×10^{-4} mol m^{-2} [50, 51] was used in both OPC experiments and later in the ICM simulation (see Section 2.3). The $\sigma_{re}(\lambda)$ value in the OPC experiment was finally determined by comparing the experimentally determined $j_{\mathrm{surface\ nitrate}}$ value and our previous laboratory-measured $\sigma_{re}(\lambda)$ value (Figure S5), the difference of which highlights the different surface nitrate densities between the OPC experiment and our previous studies. Note that the HONO production rate extrapolated to real indoor environments is not affected by the assumed surface nitrate density when the surface nitrate density in the OPC experiment matches that in real indoor environments, whether 10^{-3}, 10^{-4}, or 10^{-5} mol m^{-2}. The redshifted and enhanced absorption of surface nitrate [44] accounted for the observed HONO production with a cutoff of 425 nm, emphasizing this source with photochemical implications under visible irradiation.

The relationship among the surface nitrate reactive cross section, surface nitrate photolysis frequency, HONO production rate via surface nitrate photolysis, and

corresponding HONO production flux and accumulation rate in the OPC is summarized in Figure 1. In the OPC experiment, we measured the HONO accumulation rate and followed the OPC calculation flow (Figure 1) to validate the reactive cross section, which was measured in our previous laboratory study [44]. Alternatively, we could predict the HONO accumulation rate in the OPC based on previously reported reactive cross section values, following the ICM calculation flow (please refer to Section 2.3). The obtained $\sigma_{re}(\lambda)$ values followed the OPC calculation flow could be used to verify whether surface nitrate photolysis could reproduce the HONO accumulation rate according to the ICM calculation flow.

2.3. ICM Construction for a Simulated Room. An ICM was constructed following the calculation structure stated above facilitating either HONO budget analysis of typical indoor environments or data analysis for OPC experiments. The ICM reproduced the measured HONO accumulation rate during the OPC experiment, validating the ICM method for indoor environments.

As described in Section 2.2, γ_0, $S_{shining}/V$, $S - S_{shining}/V$, and $[NO_2]$ are major variables of $d[\mathrm{HONO}]_{NO_2}/\mathrm{dt}$. Likewise, k_{aer} is the determining factor of $d[\mathrm{HONO}]_{vent}/\mathrm{dt}$, and $I(\lambda)_{indoor}$ is important for $d[\mathrm{HONO}]_{ph}/\mathrm{dt}$ and $d[\mathrm{HONO}]_{snp}/\mathrm{dt}$. These factors were reset in the simulated room to evaluate HONO production in typical indoor environments. The dimensions of the simulated room are summarized in Table S2. The simulated room was established with an area of 15 m^2 and a ceiling height of 2.4 m, which yielded an S/V ratio of 1.9 m^{-1}, nearly 6 times lower than that of the OPC. To simplify the sunlit area calculation process of the simulated room, which is a function of the time of day, a dormant window was assumed. Therefore, the sunlit area remained constant at 15 m^2 during the day, which is much larger than the window area of 4 m^2 previously used [14]. The wall surface of the simulated room was assumed to be painted with commercial material and well-aged in the atmosphere, as is commonly encountered in real indoor environments. Filtered solar radiation via a glass window was the only light source in the daytime (06 am–06 pm) for the simulated room, and an LED lamp was the light source during the nighttime (06 pm–06 am). The outdoor solar spectrum refers to our measurements on October 5, 2020, in Beijing (Figure S3). We configured high, medium, and low transmittance values (Figure S2), which varied with the window type, as reported by Blocquet et al. [4]. A commonly used LED lamp (60 W) was the assumed indoor light source. The ventilation rate was set to approximately 0.65 h^{-1} [52], which yields a ventilation lifetime of approximately 1.54 h, slightly lower than the ventilation lifetime (~2 h) of our OPC. The ventilation lifetime setup corresponds to reality since ventilation lifetimes ranging from 0.29 to 3.45 h in fall and 0.72 to 8.33 h in winter were observed in different indoor environments in a long-term study (a median of 0.87 h in fall and 1.85 h in winter) [53]). A low ventilation rate leads to high indoor HONO accumulation in the ICM but does not change the HONO budget, which is of the highest concern in this study. $[NO_2]$ was set to 50 ppbv under all the conditions.

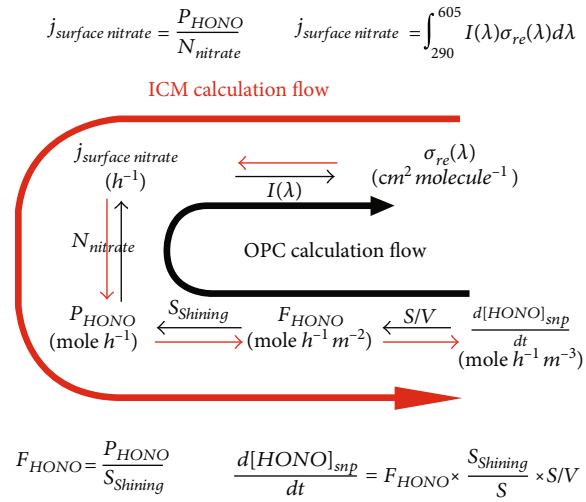

Figure 1: Relationship among the reactive cross section of surface nitrate ($\sigma_{re}(\lambda)$), photolysis frequency of surface nitrate ($j_{surface\ nitrate}$), production rate of HONO (P_{HONO}), production flux of HONO (F_{HONO}), and accumulation rate of HONO ($d[\mathrm{HONO}]_{snp}/\mathrm{dt}$) in the chamber or simulated room due to surface nitrate photolysis. In the OPC experiment, we calculated and validated the reactive cross section from the measured accumulation rate of HONO following the OPC calculation flow, while in the ICM simulation, we predicted the HONO accumulation rate and validated the indoor HONO source based on the assumption of a reactive absorption cross section.

The major HONO budget terms of the simulated room are summarized in Table 1. The indoor HONO sources included surface nitrate photolysis and photoenhanced heterogeneous reactions of NO_2 on indoor surfaces. The indoor HONO sinks included HONO ventilation and photolysis losses. Other gas-phase reactions, such as OH radical oxidation of HONO as a HONO sink and the recombination reaction between OH radicals and NO as a HONO source, are negligible and were not considered. Direct emission sources of HONO in indoor environments, such as off-gassing from indoor walls and combustion processes such as burning candles, cooking, cigarette smoking, and open fireplaces [13], were also not considered. The major HONO sources and sinks jointly determine the HONO accumulation rate in the simulated room.

Here, the ICM was employed to simulate four scenarios (S1, S2, S3, and S4) to better cover the variations in real indoor environments (Table S3). S1, S2, and S3 are scenarios involving medium-, high-, and low-transmittance glass windows [4], respectively, in a normal room, with a γ_0 value of 1×10^{-8}, similar to our OPC chamber and previously reported for living rooms and bedrooms [14]. High-transmittance glass windows and a high γ_0 value of 5×10^{-7} were set in S4 to establish a kitchen scenario. The corresponding surface nitrate photolysis rates were 2.5×10^{-7} (S1), 1.0×10^{-7} (S2), and $8.4 \times 10^{-8}\ s^{-1}$ (S3) in the daytime and $7.6 \times 10^{-9}\ s^{-1}$ at night. Previous evaluation of surface nitrate photolysis rate in the indoor environment was not directly available. By assuming surface nitrate photolysis as the only indoor HONO source and a nitrate

Table 1: Major HONO budget and typical parameter settings in the indoor photochemical model (ICM). The daytime indoor light intensity in the ICM was determined by the solar radiation and transmittance setup. The nighttime indoor light intensity in the ICM was assumed to be the same as the spectrum of LED lamps and evenly distributed. Emission sources of HONO were not considered in the ICM.

Terms	Reaction	Parameter	Model setting
HONO source	Surface HNO_3 or NO_3^-+hν ($\lambda \geq 290$ nm) ➔ HONO	$j_{\text{surface nitrate\_indoor}}$ (s^{-1})	Noontime value[a]: 2.5×10^{-7} (high), 1.0×10^{-7} (medium), 8.4×10^{-8} (low) Nighttime value: 7.6×10^{-9}
	NO_2+surface ($\lambda \geq 290$ nm) ➔ HONO	γ_0 and EF	γ_0: 1×10^{-8} (normal room), 5×10^{-7} (kitchen) Noontime EF: 6 Nighttime EF:1
HONO sink	HONO+hν ($\lambda \geq 290$ nm) ➔ OH+NO	$j_{\text{HONO\_indoor}}$ (s^{-1})	Noontime value[b]: 2.1×10^{-4} (high), 2.6×10^{-5} (medium), 5.4×10^{-7} (low)
	Ventilation	k_{aer} (h^{-1})	0.65

[a,b]The value is given based on the solar radiation recorded on October 5, 2020, at the PKU site. High, medium, and low denote the noontime $j_{\text{surface nitrate-indoor}}$ or $j_{\text{HONO-indoor}}$ levels under the high-, medium-, and low-transmittance scenarios, respectively.

surface density of 1×10^{-4} mol m^{-2}, a photolysis rate constant of $(7.3 \pm 2.3) \times 10^{-8}$ s^{-1} is calculated for the OPC experiment and is comparable to our settings. Previous measurements on the reactive cross section of surface nitrate on aerosol particle generate a much higher photolysis rate constant of $(0.7 - 2.1) \times 10^{-5}$ s^{-1} [44]. The photolysis rate of surface nitrate on painted walls under illumination of indoor lamps was estimated to be $(0.5 - 3.3) \times 10^{-9}$ s^{-1} based on the production of HONO, NO and NO_2 in the range of <0.6 ppbv in a flow cell [30]. In the absence of UV irradiation, the photolysis rate of nitrate on indoor surfaces is generally lower than that outside. The surface nitrate photolysis rate spanned over three orders of magnitude indicated the heterogeneity of indoor surface reactivity. HONO photolysis loss rates of 2.1×10^{-4} (S1), 2.6×10^{-5} (S2), and 5.4×10^{-7} s^{-1} (S3) were obtained in the daytime. These values are consistent with the peak values of 1.5×10^{-4} s^{-1} recorded in a lab room in Guangzhou, China [54] and a classroom in Marseille, France [55], and also in agreement with that value of 7.2×10^{-5} s^{-1} determined for sunlit region (around noon) in the residence in New York [13]. No HONO photolysis loss occurs at night considering the wavelength range of the LED spectrum, and ventilation is the only sink.

3. Results and Discussion

3.1. Indoor HONO Accumulation in the OPC Experiment. In the OPC experiment (October 4–7, 2020), we observed substantial variations in the HONO mixing ratio in the chamber, HONO_indoor (Figure 2(b)). HONO_indoor varied between 2.2 and 20.3 ppbv (mean = 6.3 ppbv; median = 4.1 ppbv; mode = 5.0 ppbv), whereas the ambient HONO mixing ratio, HONO_outdoor, ranged from 0.07 to 2.4 ppbv (mean = 0.7 ppbv; median = 0.5 ppbv; mode = 0.4 ppbv) during the same period. The HONO_indoor average value was approximately 10 times the HONO_outdoor average value, suggesting the presence of indoor sources, in accordance with previous studies [10, 48]. Moreover, regarding NO_2 in the chamber, NO_2_indoor varied between 6.1 and 32.5 ppbv and exhibited a similar trend to that of ambient NO_2, i.e., NO_2_outdoor. The HONO/NO_2 ratio was calculated in both the chamber (HONO/NO_2_indoor) and ambient environment (HONO/NO_2_outdoor) (Figure 2(d)). The estimated HONO/NO_2_outdoor levels (0.032 ± 0.015; median: 0.028) were comparable to previously measured outdoor ratios [48] but were much lower than the HONO/NO_2_indoor levels (0.448 ± 0.445; median: 0.206). The average HONO/NO_2_indoor is higher than the HONO/NO_2 ratio of 0.36, 0.17, 0.08, and 0.13 measured in Guangzhou lab room [54], Californian homes [56], residences at Albuquerque [57], and Toronto [10], respectively. High HONO/NO_2_indoor levels are mainly driven by fast HONO accumulation, as indicated in the time series of HONO and NO_2.

The diel variations in HONO_indoor (Figure 3(a)) revealed that the mixing ratios of HONO_indoor in the daytime were much higher (9.5 ± 5.1 ppbv; median: 8.6 ppbv) than those in the nighttime (3.1 ± 0.8 ppbv; median: 2.8 ppbv) with a maximum (16.1 ± 5.4 ppbv) at noon, whereas HONO_outdoor (Figure 3(b)) during the same period exhibited higher values in the nighttime (0.97 ± 0.59 ppbv; median: 0.86 ppbv) than those in the daytime (0.39 ± 0.50 ppbv; median: 0.24 ppbv) with a minimum (0.17 ± 0.12 ppbv) at noon. Moreover, the HONO/NO_2_indoor values in the daytime (0.755 ± 0.433; median: 0.729) were much higher than those in the nighttime (0.138 ± 0.057; median: 0.122), which further highlights greater indoor HONO accumulation in the daytime than in the nighttime. In contrast, slightly higher HONO/NO_2_outdoor values were observed in the nighttime (0.033 ± 0.015; median: 0.030) than in the daytime (0.030 ± 0.014; median: 0.027). To note, it has not been observed indoors the distinct HONO diel variations with a maximum at noon. Previous direct HONO measurements in real indoor environments with UV transmission indicated that HONO diel variations could be perturbed by its fast photolysis or impacted by other factors, such as the temperature and RH [10, 12, 58]. However, our measured HONO_indoor values were comparable

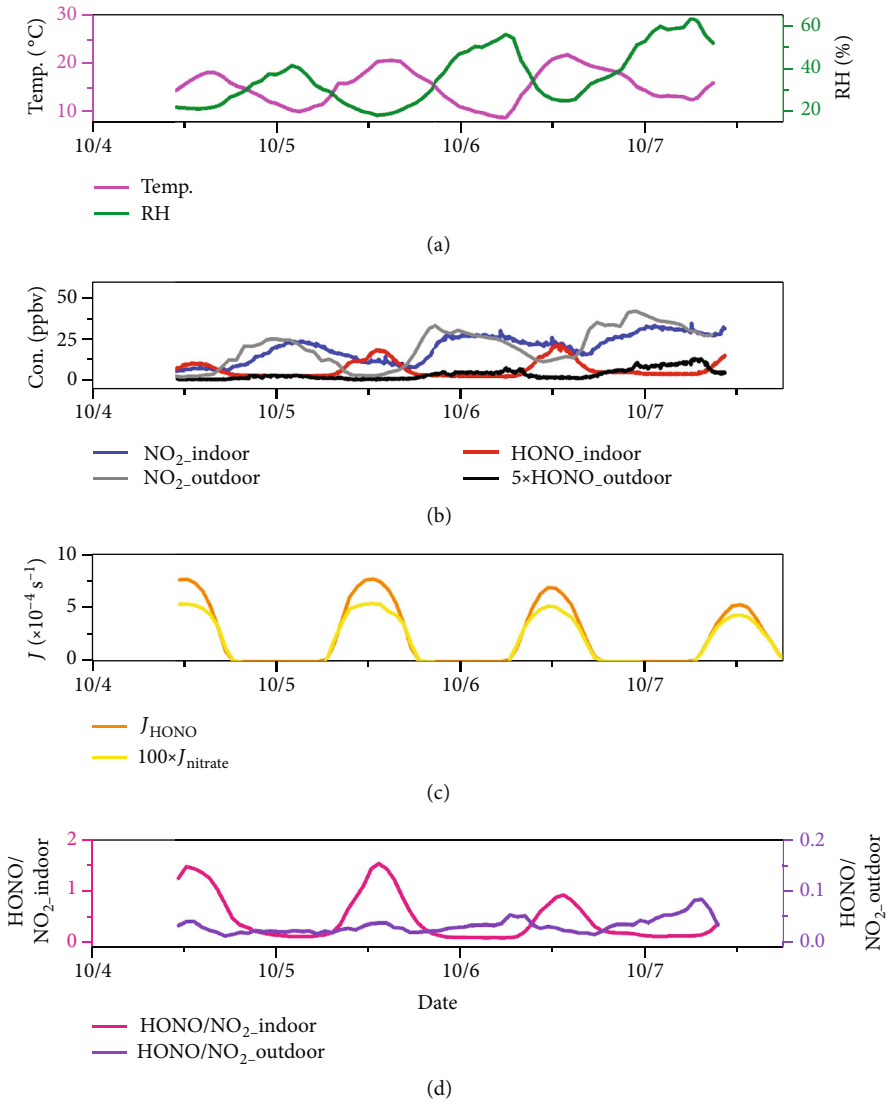

Figure 2: Trends of the temperature (Temp.), RH, HONO, NO_2, J_{HONO}, $J_{nitrate}$, and HONO/NO_2 for the OPC experiments with solar radiation as the light source from October 4–7, 2020.

overall to reported indoor values ranging from 1 to 20 ppbv for different environments or locations regardless of direct emissions stemming from combustion sources [58, 59].

Daytime HONO_indoor accumulation likely could not be attributed to NO_2 heterogeneous reactions, as HONO_indoor was largely independent of NO_2_indoor (Figure S6). A linear least-squares fit to the data revealed that HONO_indoor was weakly correlated with [NO_2], RH, and [NO_2]·RH in both the day- and nighttime ($R^2 < 0.1$, Table 2 and Figure S6). Daytime HONO_indoor accumulation was largely controlled by solar radiation. As a result, fine correlations between HONO_indoor and $[NO_2] \cdot J_{nitrate}$ ($R^2 = 0.50$) were established. Previous studies suggested that this correlation supports the photoinduced conversion of NO_2 into HONO under the illumination of UV and visible light [14–17]. In this work, OPC window-filtered solar radiation with wavelengths shorter than 425 nm and therefore excluded UV-induced conversion. Photoenhanced conversion of NO_2 into HONO under illumination of visible light on humic acid or polyphenolic films [22, 24–26] cannot be fully excluded here, although OPC chamber surface might be very different from humic acid or polyphenolic films. Correlations between HONO_indoor and $[NO_2]$ RH $J_{nitrate}$ ($R^2 = 0.12$) suggested that the photoinduced conversion of NO_2 into HONO could not be established. Particularly, data retrieved from the high- and low-NO_2 parallel experiments conducted during October 27–30, 2020 (Figure S4) in the OPC, also demonstrated that changes in NO_2_indoor ($\Delta NO_2 = 20$ ppbv) imposed a minor effect on the HONO mixing ratio (ΔHONO <1 ppbv). Daytime HONO_indoor accumulation (ΔHONO = 12 ppbv) was likely too high for any heterogeneous reaction of NO_2, especially considering minimum NO_2 mixing ratio in the daytime.

The correlations between HONO_indoor and daytime photolysis frequencies were reminiscent of the photolysis of surface nitrate [30], the indoor HONO source under

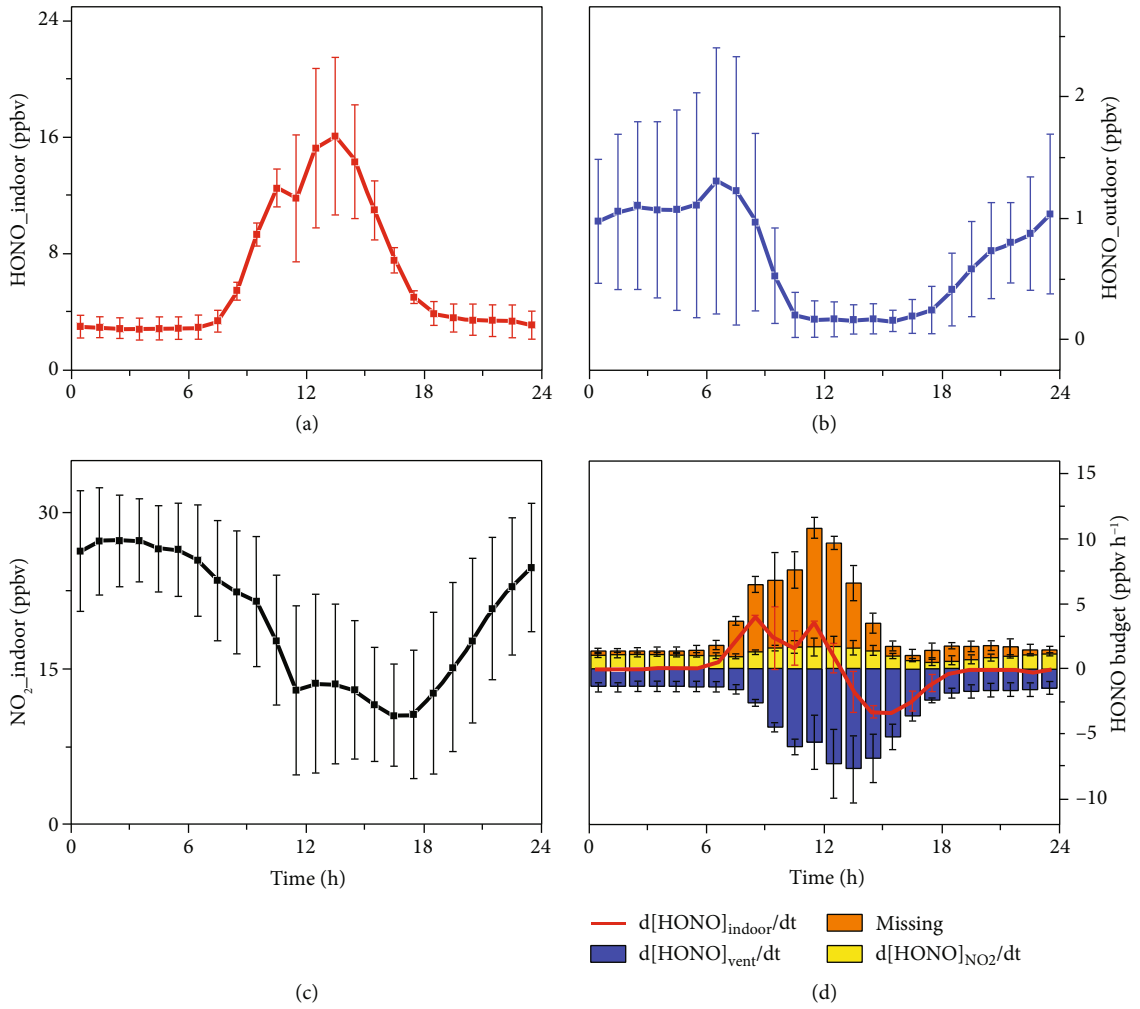

Figure 3: Diel profile of the HONO, NO_2, and HONO budgets for the OPC experiment. $d[HONO]_{NO2}/dt$ denotes the HONO source strength derived from heterogeneous NO_2 surface reactions.

Table 2: Linear correlation factors (Pearson correlation and R^2) of HONO and the missing source rate with meteorological factors and different NO_2 parameters for the OPC experiment.

	Daytime		Nighttime	
	HONO	Missing source	HONO	Missing source
Temperature	0.10	0.18	0.54	0.30
RH	0.05	-0.0002	0.03	0.02
NO_2	-0.02	0.05	0.09	0.07
NO_2·RH	-0.01	0.01	0.08	0.03
$J_{nitrate}$	0.52	0.38	—	—
NO_2·$J_{nitrate}$	0.50	0.48	—	—
NO_2·RH·$J_{nitrate}$	0.12	0.34	—	—

examination in this study. Here, $J_{nitrate}$, the enhanced photolysis rate constant of surface nitrate could be obtained (equation (16)) based on our previous measurements [44], underlining enhancement in the visible region. Even with UV filtering in the OPC, a considerable $J_{nitrate}$ value could still be obtained. In fact, a correlation between HONO_indoor and $J_{nitrate}$ ($R^2 = 0.52$) was established. Furthermore, indoor HONO accumulation was accelerated as the air quality continued to worsen over the three OPC days (Figure 2(b)). This trend might be controlled by the increase in surface nitrate, which occurs in dynamic equilibrium with gaseous HNO_3.

The nighttime measurements revealed a remarkable stability of HONO. Weaker formation and a near-steady-state

equilibrium between HONO and surface nitrite were proposed. The fine correlation between the HONO mixing ratio and temperature at night ($R^2 = 0.54$) supported this proposal [10, 12]. The weak correlation ($R^2 = 0.10$) between the HONO mixing ratio and temperature in the daytime did not necessarily preclude repartitioning between HONO and its surface reservoir but highlighted the likely strong perturbation of the indoor HONO budget by the surface photochemistry.

3.2. HONO Budget in the OPC. $d[\mathrm{HONO}]_{\mathrm{indoor}}/dt$ indicated a HONO accumulation trend as the sun rose and a HONO declining trend as the decrease of solar radiation from noon in the daytime and a flat trend in the nighttime (Figure 3(d)). Based on equations (4)–(6), the derived total HONO source exhibited a similar diel profile. Here, we focus on the daytime HONO budget and examine this indoor HONO source. Partitioning between HONO and its surface reservoir was omitted in budget analysis due to a lack of direct measurements. As a result, the nighttime HONO budget was not perfectly constrained. However, this omission should slightly affect the daytime indoor HONO budget constraints. Photochemical sources were carefully examined. The HONO sink via its reaction with OH was estimated but could be neglected (~0.4 ppbv h^{-1} at noon) assuming a daytime OH concentration of 2×10^6 molecule cm^{-3} [55]. The HONO source via the reaction between NO and OH was also negligible (~0.5 ppbv h^{-1} when NO = 7 ppbv). These two HONO budget terms were therefore not included in our model. Direct HONO photolysis was largely suppressed as a result of UV filtering in the OPC. However, HONO photolysis was included in our budget analysis to underline the sink feature of indoor HONO (equations (4)–(6)). A ventilation rate of 0.48 h^{-1} was suitably characterized in the OPC experiment and was therefore considered in budget analysis.

The contribution of NO_2 heterogeneous reactions to HONO budget depends strongly on γ_0 and EF. High- and low-NO_2 parallel experiments in our OPC were designed to estimate γ_0 and EF. Nighttime HONO production was assumed to be fully accounted by the NO_2 heterogeneous reactions, so that an upper limit of γ_0 for the OPC could be obtained. The average mixing ratio of NO_2 was 1 ppbv in the low-NO_2 experiment, much lower than the average NO_2 mixing ratio of 23 ppbv in the high-NO_2 experiment (Figure S4). HONO production based on previous measurements on NO_2 uptake coefficient could lead to significant nighttime HONO accumulation, which was however not observed (Figures 2 and S4). This immediately suggested a lower γ_0 as compared with previous reports (Table S1 and references therein [14, 15, 18–29]). An upper limit γ_0 value of 1×10^{-8} was eventually calculated for our OPC, which was at the lower end of previous measurements [14, 29]. As a matter of fact, previous measurements of γ_0, for example, on organic particles [22, 24–26], urban grime [29], and glass windows in bedrooms and living rooms under dark conditions [14], spanned across two orders of magnitude and suggested heterogeneity in the surface reactivity toward NO_2. The painted surface in our OPC did exhibit a low reactivity toward NO_2, reflecting the heterogeneity in the reactivity of OPC walls. Photoenhanced uptake of NO_2 was validated under the illumination of UV light or visible light (Table S1). The photoenhanced γ spanned over two orders of magnitude as well with an EF lower limit of roughly lower than 10 folds. Heterogeneity in the reactivity of varied surfaces justifies the span, while EF was found to be a function of NO_2 concentration, surface photosensitization reactivity, wavelength, and intensity of illuminating light etc. (Table S1). Photoenhanced γ was ranging from 10^{-6} to 10^{-5} on humic acid surfaces and was almost doubled in low-NO_2 conditions as relative to high-NO_2 conditions in flow tube reactor [24–26], while photoenhanced γ on the order of 10^{-7} on polyphenolic films was also reported in the presence of visible light [22], representing a much lower value as compared to UV illumination [26]. In our OPC experiment, visible light ($\lambda > 425$ nm) and medium range abundance of NO_2 can not ensure a high EF. In addition, the chamber wall was painted white (paint brand: Dulux) and allowed deposited aerosol particles to simulate indoor environments such as bedroom and living room. There was no additional coating of photosensitization materials, such as humic acid or polyphenolic. Finally, an estimated EF value of 6 was applied for noontime irradiation conditions according to previous studies [14] and represented an upper limit value of EF for our OPC experiments. The derived missing source of HONO based on the upper limit γ_0 and EF decreased to zero in the early morning rush hours and the afternoon rush hours (Figures 3(d) and 4(a)), confirming that contribution of NO_2 heterogeneous reactions evaluated here represented its upper limit.

Under the above assumptions and the concept of photoenhanced uptake of NO_2 by wall surfaces, the HONO source strength resulting from NO_2 heterogeneous reactions, $d[\mathrm{HONO}]_{\mathrm{NO_2}}/dt$, exhibited a distinct diel shape with a noontime maximum, as evaluated by equations (7)–(8). The enhanced daytime $d[\mathrm{HONO}]_{\mathrm{NO_2}}/dt$ value could mainly be attributed to the uptake enhancement with increasing light intensity [14], while the lower NO_2 concentration in the daytime than that in the nighttime partly could offset this enhancement. The daytime average $d[\mathrm{HONO}]_{\mathrm{NO_2}}/dt$ value of 1.09 ± 0.42 ppbv h^{-1} accounted for 22.8% of the total source rate. The missing source rate ($= d[\mathrm{HONO}]_{\mathrm{indoor}}/\mathrm{dt} + d[\mathrm{HONO}]_{\mathrm{vent}}/\mathrm{dt} - d[\mathrm{HONO}]_{\mathrm{NO_2}}/\mathrm{dt}$) exhibited a nearly identical variation to that in HONO_indoor, accounting for 77.2% of the total source rate in the daytime and 67.2% of the all-day average. The unknown source with photochemical properties was thus examined against surface nitrate photolysis, according to previous reports on indoor HONO sources [30]. One could obtain $d[\mathrm{HONO}]_{\mathrm{snp}}/\mathrm{dt}$ from surface nitrate photolysis induced by visible light using the ICM calculation flow (Figure 1) given the obtained reactive cross section (please refer to Sections 2.2 and 2.3 and Figure S5). $d[\mathrm{HONO}]_{\mathrm{snp}}/\mathrm{dt}$ indicated similar diel variations and a noontime maximum as the missing source (Figure 4). A linear least-squares fit to the data revealed that $d[\mathrm{HONO}]_{\mathrm{snp}}/\mathrm{dt}$ and the missing

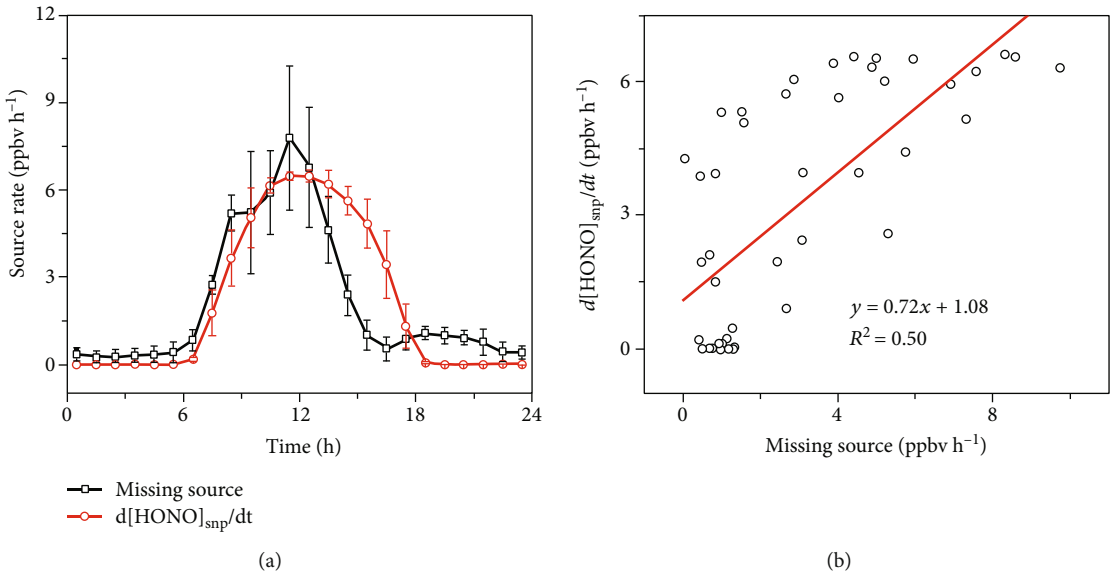

FIGURE 4: Comparison between the measured unknown source rate (Missing source) and the calculated source rate from surface nitrate photolysis (d[HONO]$_{snp}$/dt) in the OPC experiments.

source rate were suitably correlated ($R^2 = 0.50$, slope = 0.72). It could be concluded that the photolysis of surface nitrate, an indoor HONO source, mainly accounted for indoor HONO accumulation in the OPC.

3.3. Evaluation of This Indoor HONO Source in Real Indoor Environments. Direct extrapolation of this HONO source to typical residential rooms and workplaces is feasible. First, considering the OPC chamber wall surface, Dulux latex paint is widely used in room decoration. Second, the chamber glass windows can mimic room windows in terms of UV filtering. Finally, the chamber was conditioned before the experiment and ventilated with ambient air during the experiment to mimic real gas–wall interactions in actual indoor environments. The success of our model in reconstructing the HONO budget in the OPC also supports the evaluation of indoor HONO accumulation in real indoor environments.

Daily average HONO accumulation levels of 2.4, 1.6, 1.4, and 29.4 ppbv were reached under the S1, S2, S3, and S4 scenarios, respectively (Figure 5). Except for S4, these HONO values agree with the range in literature reports [55, 58] considering indoor environments free of combustion sources. The two photochemical processes on wall surfaces could therefore account for daytime HONO accumulation in typical living rooms and bedrooms. However, the rapid buildup to elevated HONO levels with maximum steady-state mixing ratios higher than 50 ppbv during cooking in kitchens [48, 60] confirms that secondary HONO formation indoors is generally less important than primary emission in kitchens.

Budget analysis suggests that the two complementary processes, i.e., heterogeneous NO_2 reactions and surface nitrate photolysis, contribute 47.3% and 52.7%, respectively, under S1, 54.1% and 45.9%, respectively, under S2, and 57.6% and 42.4%, respectively, under S3 (Figure 5). Compared to heterogeneous NO_2 reactions, HONO production resulting from surface nitrate photolysis was even stronger or at least comparable. This could be primarily attributed to the higher daytime photolysis rate constant of surface nitrate. With the noontime photolysis rate constant reaching 2.5×10^{-7}, 1.0×10^{-7}, and 8.4×10^{-8} s^{-1}, the corresponding HONO emission rates are 4.0×10^{-7}, 1.7×10^{-7}, and 1.4×10^{-7} mole h^{-1} m^{-2}, respectively, for high- (S1), medium- (S2), and low-transmittance (S3) glass windows [4] (Figure S2), respectively, in a typical living room or bedroom. The noontime indoor HONO production rate from surface nitrate photolysis are 4.1, 1.8, and 1.4 ppbv h^{-1} under S1, S2, and S3, respectively. Heterogeneous NO_2 reactions and surface nitrate photolysis contributed 95.3% and 4.7%, respectively, under S4 when the primary emission source of HONO in the kitchen was not considered. The upper limit reaction rate of NO_2 partly accounted for its higher contribution to the HONO source budget under S4. Moreover, surface nitrate photolysis strongly depends on the UV availability, which was negligible under the median- and low-transmittance conditions of S2 and S3 relative to the high-transmittance conditions of S1. As a result, surface nitrate photolysis under S2, S3 represented the lower evaluation limit. Overall, S4 simulated extreme conditions where heterogeneous NO_2 reactions are the most important factor and surface nitrate photolysis is the least important factor. The considerable contribution of surface nitrate photolysis, relative to heterogeneous NO_2 reactions, provided robust validation of this indoor HONO source (surface nitrate photolysis) in various real indoor environments.

Due to the notable dependence of surface nitrate photolysis on the UV availability, the contribution of LED light sources was negligible relative to filtered solar radiation under all transmittance conditions (Figure 5). This result

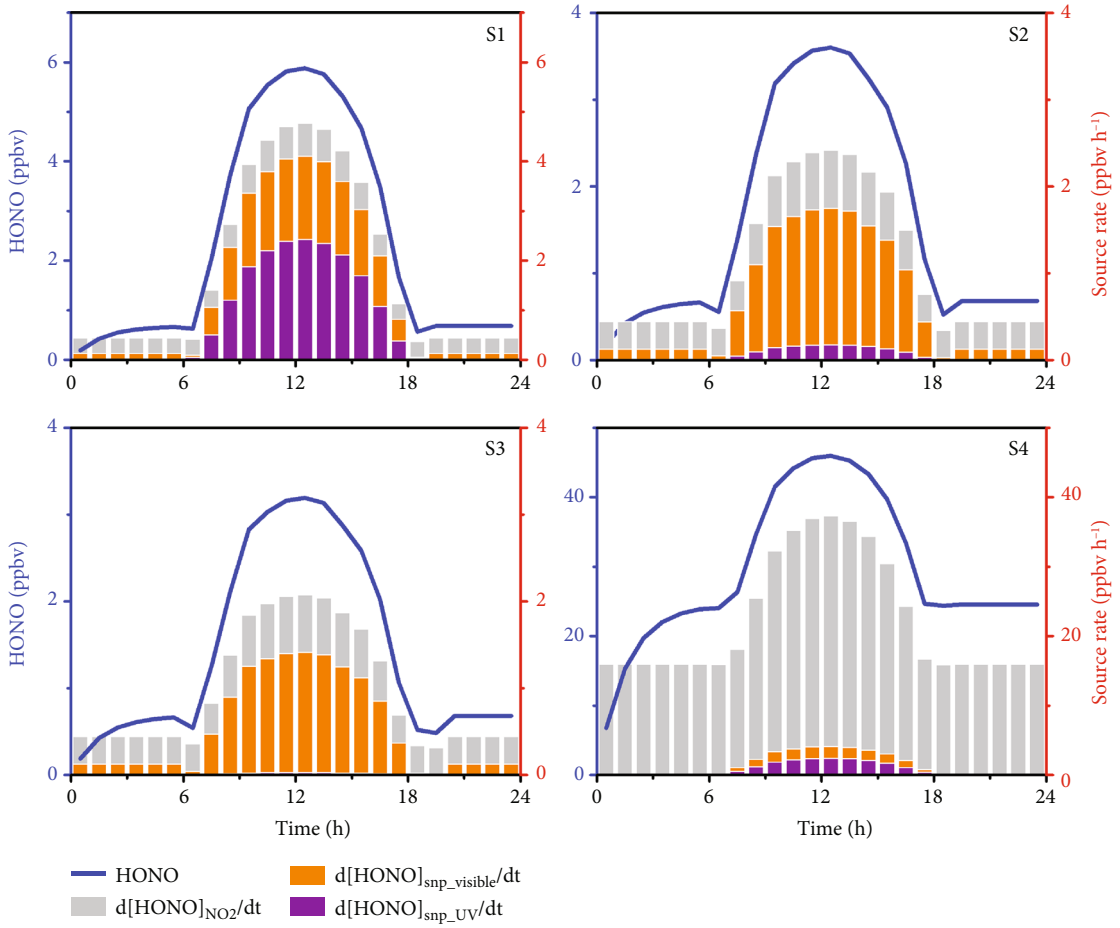

Figure 5: Indoor HONO accumulation and HONO source budget (d[HONO]$_{NO2}$/dt, d[HONO]$_{snp\_visible}$/dt, and d[HONO]$_{snp\_UV}$/dt denote the source rate derived from NO_2 surface reactions and surface nitrate photolysis in the visible and UV ranges, respectively) in typical living room (S1–S3) and kitchen (S4) environments as evaluated via the ICM calculation flow.

not only agrees with the results of previous studies [46] but also supports our OPC experiments involving LED light sources without HONO production (not shown). While solar UV light is highly important, solar visible light also contributed 35.1%, 58.9%, and 59.3% to the total daytime sources under scenarios S1, S2, and S3, respectively, due to the much higher photon density of visible light than that of UV light.

Ventilation is a simple and effective way to reduce the levels of indoor pollutants upon outdoor–indoor transport. To assess the model sensitivity and determine the ventilation rate needed to suppress indoor HONO accumulation, we modeled the maximum HONO formation around noon (from 1100 to 1300) as a function of the ventilation rate (Figure 6). The required ventilation rates to reach an outdoor average HONO level of 1.44 ppbv [61] in Beijing were 1.5 and 1.7 h^{-1} at noon under scenarios S3 and S2, respectively, with low and medium transmittance levels in the living room. Under low transmittance, a typical ventilation rate ranging from 0.1 – 4 h^{-1} [53] could lead to a noontime HONO accumulation level ranging from 14.3 – 0.5 ppbv. Under ventilation rate upper limits of 3.46 h^{-1} in fall and 1.39 h^{-1} in winter [53], noontime HONO accumulation levels could still reach up to 1.28 and 3.0 ppbv, respectively, posing a potential health threat to residents given the high transmittance in living rooms at noon. Under low-transmittance conditions, median ventilation rates of 1.15 h^{-1} in fall and 0.54 h^{-1} in winter [53] could lead to noontime HONO accumulation levels of 1.8 and 3.8 ppbv, respectively, reflecting effective management of indoor HONO accumulation. Overall, mere ventilation could insufficiently suppress indoor HONO accumulation due to photoenhanced secondary production. A low-transmittance window is highly encouraged for the sake of the health of residents.

3.4. Uncertainties. Even though we could not obtain firm conclusions regarding the exact mechanism of HONO formation, this work revealed that instantaneous heterogeneous NO_2 conversion is not the only HONO source in the OPC experiment. We propose that HONO emission results from surface nitrate photolysis, including both direct nitrate photolysis and surface catalytic reactions. Other light-dependent reactions, such as the photolysis of nitrogen compounds (e.g., humic acid), could contribute to daytime HONO accumulation [39] but were not included in our data analysis scheme for the OPC experiment. The omission of

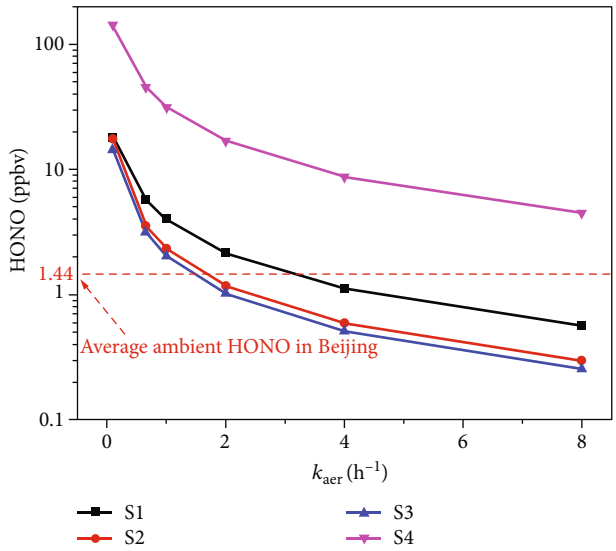

FIGURE 6: Ventilation rate needed to suppress indoor HONO accumulation around noon under the various conditions, as evaluated by the ICM calculation flow. The red dashed line denotes a certain threshold, referring to the average ambient HONO observed in Beijing [61].

equilibrium-type processes did not prevent us from successful reproduction of the HONO observation. However, equilibrium-type processes are shown to be an important HONO source or sink in real indoor environments [10, 12]. The omission of equilibrium-type processes therefore may cause the model to slightly underestimate HONO once the release of HONO from inner reservoir becomes predominant under the low HONO mixing ratios in the morning and to slightly overestimate HONO once HONO partitioning into the inner reservoir prevails under the high HONO mixing ratios in the afternoon (Figure 4). Notably, the chemical processes of surface nitrate photolysis were the key model elements, which are essential for the model to reproduce our observation in OPC.

As for the ICM evaluation of indoor HONO sources in real indoor environments, we focus on as well the two major daytime HONO sources responsible for the noontime maximum. However, under different environmental conditions, the major influencing factors could change to gas–surface partitioning affected by the temperature or heterogeneous NO_2 reactions affected by RH [58]. An increase in the HONO source derived from surface nitrate photolysis could either lead to direct HONO accumulation or surface storage as nitrite ions, which are subsequently released into the indoor environment. This behavior should be examined in a wide variety of indoor spaces. In addition, the environmental variability of the two major daytime HONO sources shall be highlighted. ICM representation of such environmental variability could be gained given future measurement constraint of these key kinetic parameters, including not only the window transmittance but also surface nitrate content, γ_0 and EF for NO_2 heterogeneous reactions, and photolysis rate constant for surface nitrate. For example, when surface nitrate content increased to be one order of magnitude large than that assumed in OPC chamber (i.e., 10^{-3} versus 10^{-4} mol m^{-2}) and γ_0 increased to be 1.0×10^{-7}, the derived noontime photolysis rate of surface nitrate is 1.0×10^{-8} s^{-1} for living rooms with medium transmittance. Thereby, the daytime accumulation of HONO is 5.3 −10.3 ppbv, with the surface nitrate photolysis and photoenhanced uptake of NO_2 accounting for 19% and 81%, respectively. ICM is therefore useful to analyze indoor HONO budget and guide future strategies to mitigate indoor air pollution. Here in the ICM model S1−S4 scenarios considering only the variability in transmittance and γ_0, nitrate photolysis was validated a new source of indoor HONO. As a result of more strong dependence of HONO photolysis on UV than surface nitrate photolysis, indoor environments filtering UV are feasible to lead to indoor HONO accumulation from surface nitrate photolysis. The relative importance of the two chemical sources of HONO, i.e., surface nitrate photolysis and heterogeneous reactions of NO_2, could also be specifically evaluated by ICM framework, given proper measurement constraint of the model.

4. Conclusions

In this work, we combined chamber experiments and model simulations to investigate the photochemical formation budget of HONO in simulated OPC and typical real indoor environments. Under UV light filtering in the OPC ($\lambda > 425$ nm), HONO accumulation substantially increased or decreased with solar irradiation, suggesting that visible light-induced processes could facilitate considerable daytime HONO production with profound implications for HONO budget analysis in indoor environments under a high photon density of visible light. Weak correlations and opposite diel profiles between HONO and NO_2 verified that heterogeneous NO_2 reactions slightly affected HONO accumulation. By applying the ICM calculation flow to determine the HONO budget in the OPC, visible light-induced photolysis of surface nitrate accounted for 77.2% of the daytime HONO formation in the chamber. Successful OPC reproduction encouraged further application of the ICM in HONO budget evaluation under high-, medium-, and low-transmittance conditions in typical living rooms and kitchens. The strength of surface nitrate photolysis was found to account for more than 60% of the total daytime HONO accumulation in a typical living room. Even under typical kitchen conditions, surface nitrate photolysis remained a considerable HONO source relative to heterogeneous reactions of NO_2 or even the total HONO source budget. The indoor HONO source derived from surface nitrate photolysis was thus consistently validated between our OPC and ICM evaluations.

While surface nitrate photolysis strongly depends on the UV availability, visible light also accounts for 35.1–59.3% of the total daytime HONO production resulting from surface nitrate photolysis. Ventilation cannot effectively dilute the indoor HONO source of a photoenhanced nature around noontime. Window glass with a low or no light transmission in the UV range could greatly suppress secondary indoor HONO production and is highly recommended considering the health of residents.

Data Availability

Data are available upon reasonable request to the corresponding author.

Conflicts of Interest

The authors declare no competing financial interests.

Authors' Contributions

Youfeng Wang conducted the experiments, carried out the data analysis, and wrote the manuscript. Chunxiang Ye designed this study, supervised the analysis, and revised the manuscript. Chong Zhang and Jianshu Wang provided some data. All authors participated in the interpretation of results and helped to improve the manuscript.

Acknowledgments

This work was funded by the National Natural Science Foundation of China (Grant Nos. 42175120 and 91744206) and the China Postdoctoral Science Foundation (Grant No. 2019 M650353).

Supplementary Materials

Figure S1: configuration of the outdoor photochemical chamber (OPC) at the PKU site; the inlet tube was used to pass the low-NO_2 air or high-NO_2 air into the chamber during Oct. 27–30, 2020. Figure S2: transmittance of the glass filter used for the outdoor photochemical chamber (OPC) and high-, medium-, and low-transmittance setup for the indoor photochemical model (ICM). Figure S3: outdoor solar flux measured in Beijing on 12 : 30, October 5, 2020, and LED flux for the indoor photochemical model (ICM). Figure S4: time series of HONO and NO_2 mixing ratios in "low-NO_2" (daytime on Oct. 27 and 28) and "high-NO_2 air" (daytime on Oct. 29) OPC experiments. Figure S5: the reactive cross section ($\sigma_{re}(\lambda)$) obtained by comparing the $j_{surface\,nitrate}$ between the OPC experiment and our previous laboratory-measured $\sigma_{re}(\lambda)$ [44]. Figure S6: correlation of HONO concentration in the outdoor photochemical chamber (HONO_indoor) with NO_2 (NO_2_indoor), $J_{nitrate}$, RH, and temperature (Temp.) during the night (plot in black circle) and day (plot in red square), respectively. $J_{nitrate}$ was calculated based on the measured solar flux, glass transmittance, and reactive cross-section of surface nitrate [44] assuming an average surface nitrate density (1×10^{-4} mole m^{-2}) [50, 51]. Figure S7: diel profiles of ambient temperature (Temp.) and relative humidity (RH) and their respective correlation with the unknown source rate of HONO (missing source) during the OPC experiments. Table S1: overview of photoenhanced uptake coefficients (γ) of heterogeneous NO_2 reactions to produce HONO on various surfaces. Table S2: summary of the setup of the outdoor photochemical chamber (OPC) and simulated room in our constructed indoor photochemical model (ICM). Table S3: summary for scenarios considered in the outdoor photochemical chamber (OPC) experiment and indoor photochemical model (ICM). *(Supplementary Materials)*

References

[1] N. E. Klepeis, W. C. Nelson, W. R. Ott et al., "The National Human Activity Pattern Survey (NHAPS): a resource for assessing exposure to environmental pollutants," *Journal of Exposure Science & Environmental Epidemiology*, vol. 11, no. 3, pp. 231–252, 2001.

[2] Y. Liu, A. G. Be, V. W. Or, M. R. Alves, V. H. Grassian, and F. M. Geiger, "Challenges and opportunities in molecular-level indoor surface chemistry and physics," *Cell Reports Physical Science*, vol. 1, no. 11, article 100256, 2020.

[3] A. Manuja, J. Ritchie, K. Buch et al., "Total surface area in indoor environments," *Environmental Science: Processes & Impacts*, vol. 21, no. 8, pp. 1384–1392, 2019.

[4] M. Blocquet, F. Guo, M. Mendez et al., "Impact of the spectral and spatial properties of natural light on indoor gas-phase chemistry: experimental and modeling study," *Indoor Air*, vol. 28, no. 3, pp. 426–440, 2018.

[5] A. Gandolfo, V. Gligorovski, V. Bartolomei et al., "Spectrally resolved actinic flux and photolysis frequencies of key species within an indoor environment," *Building and Environment*, vol. 109, pp. 50–57, 2016.

[6] Y. Liu, P. K. Misztal, C. Arata, C. J. Weschler, W. W. Nazaroff, and A. H. Goldstein, "Observing ozone chemistry in an occupied residence," *Proceedings of the National Academy of Sciences of the United States of America*, vol. 118, no. 6, 2021.

[7] M. Zhang, J. Xiong, Y. Liu, P. K. Misztal, and A. H. Goldstein, "Physical-chemical coupling model for characterizing the reaction of ozone with squalene in realistic indoor environments," *Environmental Science & Technology*, vol. 55, no. 3, pp. 1690–1698, 2021.

[8] D. M. Lunderberg, Y. Liu, P. K. Misztal et al., "Intake fractions for volatile organic compounds in two occupied California residences," *Environmental Science & Technology Letters*, vol. 8, no. 5, pp. 386–391, 2021.

[9] D. M. Lunderberg, P. K. Misztal, Y. Liu et al., "High-resolution exposure assessment for volatile organic compounds in two California residences," *Environmental Science & Technology*, vol. 55, no. 10, pp. 6740–6751, 2021.

[10] D. B. Collins, R. F. Hems, S. Zhou et al., "Evidence for gas–surface equilibrium control of indoor nitrous acid," *Environmental Science & Technology*, vol. 52, no. 21, pp. 12419–12427, 2018.

[11] J. Qiu, D. Xie, Y. Li et al., "Dibasic esters observed as potential emerging indoor air pollutants in new apartments in Beijing, China," *Environmental Science & Technology Letters*, vol. 8, no. 6, pp. 445–450, 2021.

[12] C. Wang, D. B. Collins, C. Arata et al., "Surface reservoirs dominate dynamic gas-surface partitioning of many indoor air constituents," *Science Advances*, vol. 6, no. 8, 2020.

[13] S. Zhou, C. J. Young, T. C. VandenBoer, S. F. Kowal, and T. F. Kahan, "Time-resolved measurements of nitric oxide, nitrogen dioxide, and nitrous acid in an occupied New York home," *Environmental Science & Technology*, vol. 52, no. 15, pp. 8355–8364, 2018.

[14] J. Liu, H. Deng, P. S. J. Lakey et al., "Unexpectedly high indoor HONO concentrations associated with photochemical NO_2 transformation on glass windows," *Environmental Science & Technology*, vol. 54, no. 24, pp. 15680–15688, 2020.

[15] E. Gomez Alvarez, M. Soergel, S. Gligorovski et al., "Light-induced nitrous acid (HONO) production from NO_2

heterogeneous reactions on household chemicals," *Atmospheric Environment*, vol. 95, pp. 391–399, 2014.

[16] V. Bartolomei, M. Soergel, S. Gligorovski et al., "Formation of indoor nitrous acid (HONO) by light-induced NO_2 heterogeneous reactions with white wall paint," *Environmental Science and Pollution Research*, vol. 21, no. 15, pp. 9259–9269, 2014.

[17] A. Gandolfo, V. Bartolomei, E. Gomez Alvarez et al., "The effectiveness of indoor photocatalytic paints on NO_x and HONO levels," *Applied Catalysis B: Environmental*, vol. 166-167, pp. 84–90, 2015.

[18] R. J. Gustafsson, A. Orlov, P. T. Griffiths, R. A. Cox, and R. M. Lambert, "Reduction of NO_2 to nitrous acid on illuminated titanium dioxide aerosol surfaces: implications for photocatalysis and atmospheric chemistry," *Chemical Communications*, vol. 37, no. 37, pp. 3936–3938, 2006.

[19] M. E. Monge, B. D'Anna, L. Mazri et al., "Light changes the atmospheric reactivity of soot," *Proceedings of the National Academy of Sciences*, vol. 107, no. 15, pp. 6605–6609, 2010.

[20] R. Ammar, M. E. Monge, C. George, and B. D'Anna, "Photoenhanced NO_2 loss on simulated urban grime," *ChemPhysChem*, vol. 11, no. 18, pp. 3956–3961, 2010.

[21] M. Brigante, D. Cazoir, B. D'Anna, C. George, and D. J. Donaldson, "Photoenhanced uptake of NO_2 by pyrene solid films," *The Journal of Physical Chemistry A*, vol. 112, no. 39, pp. 9503–9508, 2008.

[22] Y. Sosedova, A. Rouviere, T. Bartels-Rausch, and M. Ammann, "UVA/Vis-induced nitrous acid formation on polyphenolic films exposed to gaseous NO_2," *Photochemical & Photobiological Sciences*, vol. 10, no. 10, pp. 1680–1690, 2011.

[23] C. George, R. S. Strekowski, J. Kleffmann, K. Stemmler, and M. Ammann, "Photoenhanced uptake of gaseous NO_2 on solid organic compounds: a photochemical source of HONO?," *Faraday Discussions*, vol. 130, pp. 195–210, 2005.

[24] K. Stemmler, M. Ammann, C. Donders, J. Kleffmann, and C. George, "Photosensitized reduction of nitrogen dioxide on humic acid as a source of nitrous acid," *Nature*, vol. 440, no. 7081, pp. 195–198, 2006.

[25] K. Stemmler, M. Ndour, Y. Elshorbany et al., "Light induced conversion of nitrogen dioxide into nitrous acid on submicron humic acid aerosol," *Atmospheric Chemistry and Physics*, vol. 7, no. 16, pp. 4237–4248, 2007.

[26] C. Han, W. Yang, Q. Wu, H. Yang, and X. Xue, "Heterogeneous photochemical conversion of NO_2 to HONO on the humic acid surface under simulated sunlight," *Environmental Science & Technology*, vol. 50, no. 10, pp. 5017–5023, 2016.

[27] A. Gandolfo, L. Rouyer, H. Wortham, and S. Gligorovski, "The influence of wall temperature on NO_2 removal and HONO levels released by indoor photocatalytic paints," *Applied Catalysis B: Environmental*, vol. 209, pp. 429–436, 2017.

[28] J. Liu, S. Li, M. Mekic et al., "Photoenhanced uptake of NO_2 and HONO formation on real urban grime," *Environmental Science & Technology Letters*, vol. 6, no. 7, pp. 413–417, 2019.

[29] C. Yu, Z. Wang, Q. Ma, L. Xue, C. George, and T. Wang, "Measurement of heterogeneous uptake of NO_2 on inorganic particles, sea water and urban grime," *Journal of Environmental Sciences*, vol. 106, pp. 124–135, 2021.

[30] H. Schwartz-Narbonne, S. H. Jones, and D. J. Donaldson, "Indoor lighting releases gas phase nitrogen oxides from indoor painted surfaces," *Environmental Science & Technology Letters*, vol. 6, no. 2, pp. 92–97, 2019.

[31] C. S. Blaszczak-Boxe and A. Saiz-Lopez, "Nitrate photolysis in ice and snow: a critical review of its multiphase chemistry," *Atmospheric Environment*, vol. 193, pp. 224–241, 2018.

[32] C. Ye, H. Gao, N. Zhang, and X. Zhou, "Photolysis of nitric acid and nitrate on natural and artificial surfaces," *Environmental Science & Technology*, vol. 50, no. 7, pp. 3530–3536, 2016.

[33] C. Ye, N. Zhang, H. Gao, and X. Zhou, "Photolysis of particulate nitrate as a source of HONO and NO_x," *Environmental Science & Technology*, vol. 51, no. 12, pp. 6849–6856, 2017.

[34] F. Bao, M. Li, Y. Zhang, C. Chen, and J. Zhao, "Photochemical aging of Beijing urban $PM_{2.5}$: HONO production," *Environmental Science & Technology*, vol. 52, no. 11, pp. 6309–6316, 2018.

[35] A. M. Baergen and D. Donaldson, "Photochemical renoxification of nitric acid on real urban grime," *Environmental Science & Technology*, vol. 47, no. 2, pp. 815–820, 2013.

[36] A. M. Baergen and D. J. Donaldson, "Formation of reactive nitrogen oxides from urban grime photochemistry," *Atmospheric Chemistry and Physics*, vol. 16, no. 10, pp. 6355–6363, 2016.

[37] C. Ye, N. Zhang, H. Gao, and X. Zhou, "Matrix effect on surface-catalyzed photolysis of nitric acid," *Scientific Reports*, vol. 9, no. 1, p. 4351, 2019.

[38] F. Bao, H. Jiang, Y. Zhang et al., "The key role of sulfate in the photochemical renoxification on real $PM_{2.5}$," *Environmental Science & Technology*, vol. 54, no. 6, pp. 3121–3128, 2020.

[39] W. Yang, C. Han, H. Yang, and X. Xue, "Significant HONO formation by the photolysis of nitrates in the presence of humic acids," *Environmental Pollution*, vol. 243, no. Part A, pp. 679–686, 2018.

[40] O. Svoboda, L. Kubelova, and P. Slavicek, "Enabling forbidden processes: quantum and solvation enhancement of nitrate anion UV absorption," *The Journal of Physical Chemistry A*, vol. 117, no. 48, pp. 12868–12877, 2013.

[41] C. Zhu, B. Xiang, L. Zhu, and R. Cole, "Determination of absorption cross sections of surface-adsorbed HNO_3 in the 290–330nm region by Brewster angle cavity ring-down spectroscopy," *Chemical Physics Letters*, vol. 458, no. 4-6, pp. 373–377, 2008.

[42] J. Du and L. Zhu, "Quantification of the absorption cross sections of surface-adsorbed nitric acid in the 335–365nm region by Brewster angle cavity ring-down spectroscopy," *Chemical Physics Letters*, vol. 511, no. 4-6, pp. 213–218, 2011.

[43] M. Sangwan, W. R. Stockwell, D. Stewart, and L. Zhu, "Absorption of near UV light by HNO_3/NO_3^- on sapphire surfaces," *Journal of Physical Chemistry A*, vol. 120, no. 18, pp. 2877–2884, 2016.

[44] Y. Wang, J. Wang, Y. Wang et al., "Experimental and kinetic model evaluation of HONO production from surface nitrate photolysis," *Atmospheric Environment*, vol. 296, article 119568, 2023.

[45] J. Stutz, E. S. Kim, U. Platt, P. Bruno, C. Perrino, and A. Febo, "UV-visible absorption cross sections of nitrous acid," *Journal of Geophysical Research-Atmospheres*, vol. 105, no. D11, pp. 14585–14592, 2000.

[46] S. F. Kowal, S. R. Allen, and T. F. Kahan, "Wavelength-resolved photon fluxes of indoor light sources: implications for HO_x production," *Environmental Science & Technology*, vol. 51, no. 18, pp. 10423–10430, 2017.

[47] http://satellite.mpic.de/spectral_atlas.

[48] C. Wang, B. Bottorff, E. Reidy et al., "Cooking, bleach cleaning, and air conditioning strongly impact levels of HONO in a house," *Environmental Science & Technology*, vol. 54, no. 21, pp. 13488–13497, 2020.

[49] A. Depoorter, C. Kalalian, C. Emmelin, C. Lorentz, and C. George, "Indoor heterogeneous photochemistry of furfural drives emissions of nitrous acid," *Indoor Air*, vol. 31, no. 3, pp. 682–692, 2021.

[50] H. Schwartz-Narbonne and D. J. Donaldson, "Water uptake by indoor surface films," *Scientific Reports*, vol. 9, no. 1, article 11089, 2019.

[51] A. M. Baergen and D. J. Donaldson, "Seasonality of the water-soluble inorganic ion composition and water uptake Behavior of urban grime," *Environmental Science & Technology*, vol. 53, no. 10, pp. 5671–5677, 2019.

[52] L. A. Wallace, S. J. Emmerich, and C. Howard-Reed, "Continuous measurements of air change rates in an occupied house for 1 year: the effect of temperature, wind, fans, and windows," *Journal of Exposure Analysis and Environmental Epidemiology*, vol. 12, no. 4, pp. 296–306, 2002.

[53] Y. You, C. Niu, J. Zhou et al., "Measurement of air exchange rates in different indoor environments using continuous CO_2 sensors," *Journal of Environmental Sciences*, vol. 24, no. 4, pp. 657–664, 2012.

[54] J. Liu, S. Li, J. Zeng et al., "Assessing indoor gas phase oxidation capacity through real-time measurements of HONO and NO_x in Guangzhou, China," *Environmental Science: Processes & Impacts*, vol. 21, no. 8, pp. 1393–1402, 2019.

[55] E. Gomez Alvarez, D. Amedro, C. Afif et al., "Unexpectedly high indoor hydroxyl radical concentrations associated with nitrous acid," *Proceedings of the National Academy of Sciences*, vol. 110, no. 33, pp. 13294–13299, 2013.

[56] K. Lee, X. P. Xue, A. S. Geyh et al., "Nitrous acid, nitrogen dioxide, and ozone concentrations in residential environments," *Environmental Health Perspectives*, vol. 110, no. 2, pp. 145–150, 2002.

[57] J. D. Spengler, M. Brauer, J. M. Samet, and W. E. Lambert, "Nitrous acid in Albuquerque, New Mexico, homes," *Environmental Science & Technology*, vol. 27, no. 5, pp. 841–845, 1993.

[58] Y. Chen, W. Wang, C. Lian et al., "Evaluation and impact factors of indoor and outdoor gas-phase nitrous acid under different environmental conditions," *Journal of Environmental Sciences*, vol. 95, pp. 165–171, 2020.

[59] S. Gligorovski, "Nitrous acid (HONO): an emerging indoor pollutant," *Journal of Photochemistry and Photobiology A: Chemistry*, vol. 314, pp. 1–5, 2016.

[60] M. Brauer, P. B. Ryan, H. H. Suh et al., "Measurements of nitrous acid inside two research houses," *Environmental Science & Technology*, vol. 24, no. 10, pp. 1521–1527, 1990.

[61] J. Wang, X. Zhang, J. Guo, Z. Wang, and M. Zhang, "Observation of nitrous acid (HONO) in Beijing, China: seasonal variation, nocturnal formation and daytime budget," *Science of the Total Environment*, vol. 587-588, pp. 350–359, 2017.